

First-Principles Electronic Structure of Superconductor $\text{Ca}_4\text{Al}_2\text{O}_6\text{Fe}_2\text{P}_2$: Comparison with LaFePO and $\text{Ca}_4\text{Al}_2\text{O}_6\text{Fe}_2\text{As}_2$

Taichi Kosugi¹, Takashi Miyake^{1,2,3}, and Shoji Ishibashi^{1,3}

¹Nanosystem Research Institute (NRI) "RICS", AIST, 1-1-1 Umezono, Tsukuba 305-8568, Japan

²Japan Science and Technology Agency, CREST, 4-1-8 Honcho, Kawaguchi, Saitama 332-0012, Japan

³Japan Science and Technology Agency, TRIP, 5 Sanbancho, Chiyoda, Tokyo 102-0075, Japan

We investigate the electronic structures of iron-based superconductors having perovskite-like blocking layers, $\text{Ca}_4\text{Al}_2\text{O}_6\text{Fe}_2\text{P}_2$ and $\text{Ca}_4\text{Al}_2\text{O}_6\text{Fe}_2\text{As}_2$, from first principles. $\text{Ca}_4\text{Al}_2\text{O}_6\text{Fe}_2\text{P}_2$ is found to have two hole-like Fermi surfaces around Γ , and one hole-like Fermi surface around M in the unfolded Brillouin zone. This is in contrast with LaFePO , where no Fermi surface is found around M . The relationship between their band structures and measured transition temperatures of superconductivity is discussed. The number of Fermi surfaces in $\text{Ca}_4\text{Al}_2\text{O}_6\text{Fe}_2\text{P}_2$ is also different from that in $\text{Ca}_4\text{Al}_2\text{O}_6\text{Fe}_2\text{As}_2$, in which only one Fermi surface is formed around Γ . Analysis using maximally localized Wannier functions clarifies that the differences between their band structures originate mainly from the difference in pnictogen height. We then analyze the alloying effect on the electronic structure of $\text{Ca}_4\text{Al}_2\text{O}_6\text{Fe}_2\text{AsP}$. It is found that this electronic structure is similar to those of $\text{Ca}_4\text{Al}_2\text{O}_6\text{Fe}_2\text{P}_2$ and $\text{Ca}_4\text{Al}_2\text{O}_6\text{Fe}_2\text{As}_2$ with average crystal structures, though $\text{Ca}_4\text{Al}_2\text{O}_6\text{Fe}_2\text{AsP}$ contains pnictogen height disorder. We calculate the generalized susceptibility for $\text{Ca}_4\text{Al}_2\text{O}_6\text{Fe}_2(\text{As}_{1-x}\text{P}_x)_2$ and clarify the factors determining its tendency.

KEYWORDS: Fe-based superconductor, $\text{Ca}_4\text{Al}_2\text{O}_6\text{Fe}_2\text{P}_2$, $\text{Ca}_4\text{Al}_2\text{O}_6\text{Fe}_2\text{As}_2$, LaFePO , electronic structure, first-principles calculation, maximally localized Wannier function

1. Introduction

Since the discovery of iron-based superconductors in LaFePO with its transition temperature T_c of 5 K¹⁾ and in LaFeAsO with $T_c = 26$ K,²⁾ many attempts to clarify the material properties and to realize higher T_c have been continued, and Fe-based superconductors with various chemical formulae and crystal structures have been reported, among which SmFeAsO has shown the highest T_c of 55 K to date is realized.³⁾

An Fe-based superconductor comprises two-dimensional iron (Fe)-anion (A) layers. The electronic bands near the Fermi level have a strong Fe d character,⁴⁻⁷⁾ which should be responsible for the superconductivity. Lee *et al.*⁸⁾ plotted the T_c of various Fe-based superconductors as a function of the A -Fe- A bond angle α and demonstrated that the T_c shows a peak at nearly 109.47°, for which FeA_4 forms a regular tetrahedron. Much attention has thus been paid to the strong correlation between T_c and the local geometry of an FeA_4 tetrahedron, namely, the lattice constant a , the Fe- A bond length d , the bond angle α , and the anion height h_A . Two of these four geometry constants are independent. A small a or d leads to a small density of states at the Fermi level and is thus expected to be unfavorable for superconductivity. On the other hand, a large h_A allows a robust hole Fermi surface around (π, π) ,⁹⁾ which interacts with electron Fermi surfaces and is thus expected to be favorable for superconductivity.¹⁰⁾ The measured T_c 's, however, are not necessarily higher at larger h_A 's. Mizuguchi and coworkers^{11, 12)} provided a plot of T_c as a function of h_A , which obeys a symmetric curve with a peak at approximately 1.38 Å, common to

1111-, 122-, 111-, and 11-type superconductors.

Since the reports for $\text{Sr}_4\text{Sc}_2\text{O}_6\text{Fe}_2\text{P}_2$ ¹³⁾ and $\text{Sr}_4\text{V}_2\text{O}_6\text{Fe}_2\text{As}_2$,¹⁴⁾ Fe-based materials with perovskite-type blocking layers have been known to show superconductivity for various combinations of their formulae and thickness.¹⁵⁻²³⁾ They include $\text{Ca}_4\text{Al}_2\text{O}_6\text{Fe}_2\text{As}_2$ ($a = 3.713$ Å and $c = 15.407$ Å, $\alpha = 102.13^\circ$, and $h_{\text{As}} = 1.500$ Å) with $T_c = 28.3$ K²⁰⁾ and $\text{Ca}_4\text{Al}_2\text{O}_6\text{Fe}_2\text{P}_2$ ($a = 3.692$ Å and $c = 14.934$ Å, $\alpha = 109.45^\circ$, and $h_{\text{P}} = 1.306$ Å) with $T_c = 17.1$ K.²⁰⁾

Among the Fe-based superconductors reported so far, $\text{Ca}_4\text{Al}_2\text{O}_6\text{Fe}_2\text{As}_2$ and $\text{Ca}_4\text{Al}_2\text{O}_6\text{Fe}_2\text{P}_2$ are of particular interest since they have rather small a 's, owing to the small ion radius of Al^{3+} , and $\text{Ca}_4\text{Al}_2\text{O}_6\text{Fe}_2\text{As}_2$ has a rather large h_{As} . Furthermore, it is important to answer why the T_c of $\text{Ca}_4\text{Al}_2\text{O}_6\text{Fe}_2\text{P}_2$ is higher than that of LaFePO to elucidate the mechanism of superconductivity in systems consisting of FeP layers. Our previous work²⁴⁾ revealed that α has a strong impact on the band rearrangement and the Fermi surface topology in $\text{Ca}_4\text{Al}_2\text{O}_6\text{Fe}_2\text{As}_2$. Subsequently, Usui and Kuroki²⁵⁾ pointed out that the superconductivity of an Fe-based superconductor is optimized for α of a regular tetrahedron, which maximizes the hole Fermi surface multiplicity.

The superconducting properties of Fe-based systems depend sensitively on multiple factors related to the crystal structure and formula, as outlined above. It is thus important to investigate the electronic properties of such systems with the crystal structure and/or formula varied, focusing on the behavior of Fermi surfaces and electronic orbitals in the vicinity of the Fermi level. In the present

study, we therefore perform first-principles electronic structure calculations for $\text{Ca}_4\text{Al}_2\text{O}_6\text{Fe}_2(\text{As}_{1-x}\text{P}_x)_2$. We first compare the band structures of $\text{Ca}_4\text{Al}_2\text{O}_6\text{Fe}_2\text{P}_2$ and $\text{Ca}_4\text{Al}_2\text{O}_6\text{Fe}_2\text{As}_2$, and determine the origins of the differences in their band structures by comparing the transfer integrals between localized electronic orbitals. We extract the transfer integrals by constructing maximally localized Wannier functions,²⁶⁾ which provide a picture of localized electronic orbitals in solid. The results of this analysis suggest that the band structures of $\text{Ca}_4\text{Al}_2\text{O}_6\text{Fe}_2(\text{As}_{1-x}\text{P}_x)_2$ are determined mainly by crystal structure, not by chemical composition. We then demonstrate that electronic structure calculation for $\text{Ca}_4\text{Al}_2\text{O}_6\text{Fe}_2\text{AsP}$ corroborates this idea by unfolding its band structure. We calculate the generalized susceptibility χ_0 , which correlates with superconductivity in general, of $\text{Ca}_4\text{Al}_2\text{O}_6\text{Fe}_2(\text{As}_{1-x}\text{P}_x)_2$ and clarify the factors determining the behavior of χ_0 .

2. Computational Details

We used the computational code QMAS²⁷⁾ based on the projector augmented-wave method,²⁸⁾ which has been applied to the study of the ground state properties of LaFeAsO ,^{6,29)} SrFe_2As_2 ,³⁰⁾ and $\text{Ca}_4\text{Al}_2\text{O}_6\text{Fe}_2\text{As}_2$.²⁴⁾ The PBE exchange-correlation functional³¹⁾ within the generalized gradient approximation (GGA) was adopted. The pseudo wave functions were expanded in plane waves with an energy cutoff of 40 Ry. We employed a $12 \times 12 \times 4$ k point mesh for systems with conventional tetragonal cells and an $8 \times 8 \times 4$ k point mesh with supercells. The electronic band structure in the vicinity of the Fermi level is analyzed in detail using the maximally localized Wannier function technique.²⁶⁾

For the $\text{Ca}_4\text{Al}_2\text{O}_6\text{Fe}_2\text{P}_2$ ^{20,32)} and $\text{Ca}_4\text{Al}_2\text{O}_6\text{Fe}_2\text{As}_2$ ²⁰⁾ crystal structures, the experimental values of tetragonal lattice constants and atomic coordinates are used in the present work.

In the analyses of the alloying effect on $\text{Ca}_4\text{Al}_2\text{O}_6\text{Fe}_2\text{AsP}$, we unfold its band dispersion obtained for a supercell, following the procedures proposed by Ku *et al.*³³⁾ The unfolded band dispersion is given as a sum of weighted delta functions:

$$A_{kn, kn}(\omega) = \sum_J |\langle kn|KJ\rangle|^2 \delta(\omega - \varepsilon_{KJ}), \quad (1)$$

where K is the wave vector in the folded Brillouin zone corresponding to the wave vector k in the unfolded Brillouin zone. J is the band index for the supercell and n denotes the Wannier function in the primitive cell. $|KJ\rangle$ is the eigenstate of the Kohn-Sham Hamiltonian for the supercell, whereas $|kn\rangle$ is the Fourier transform of the Wannier function in the primitive cell. We are able to unfold 20 Fe d bands to 5 bands by choosing the proper gauge of the Wannier functions.⁷⁾

We calculate the generalized susceptibility χ_0 of $\text{Ca}_4\text{Al}_2\text{O}_6\text{Fe}_2\text{P}_2$ and $\text{Ca}_4\text{Al}_2\text{O}_6\text{Fe}_2\text{As}_2$ with gradually varying their crystal structures. Its expression for a sys-

tem with time reversal symmetry is given by

$$\chi_0(\mathbf{q}) = \frac{1}{2} \sum_{m,n,\mathbf{k}} \frac{f_{m\mathbf{k}} - f_{n\mathbf{k}+\mathbf{q}}}{\varepsilon_{n\mathbf{k}+\mathbf{q}} - \varepsilon_{m\mathbf{k}}}, \quad (2)$$

where $f_{m\mathbf{k}}$ is the occupation number and $\varepsilon_{m\mathbf{k}}$ is the energy eigenvalue. χ_0 reflects the nesting property of the system and is expected to correlate with superconductivity. We evaluate eq. (2) as a summation for $40 \times 40 \times 4$ k points by interpolating the band dispersion using the Wannier functions of Fe d bands.

3. Results and Discussion

3.1 Electronic properties of $\text{Ca}_4\text{Al}_2\text{O}_6\text{Fe}_2\text{P}_2$ in comparison with those of $\text{Ca}_4\text{Al}_2\text{O}_6\text{Fe}_2\text{As}_2$

The nonmagnetic electronic band structures of $\text{Ca}_4\text{Al}_2\text{O}_6\text{Fe}_2\text{P}_2$ and $\text{Ca}_4\text{Al}_2\text{O}_6\text{Fe}_2\text{As}_2$ obtained with the first-principles calculation are shown as circles in Fig. 1(a). In each of the systems, the unit cell contains two Fe atoms and ten bands having a strong Fe d character lie near the Fermi level. The most prominent difference in the calculated band structure between these two systems is the multiplicity of Fermi surfaces around Γ : $\text{Ca}_4\text{Al}_2\text{O}_6\text{Fe}_2\text{P}_2$ has three, whereas $\text{Ca}_4\text{Al}_2\text{O}_6\text{Fe}_2\text{As}_2$ has two. We note here that LaFePO has two Fermi surfaces around Γ , which would explain why $\text{Ca}_4\text{Al}_2\text{O}_6\text{Fe}_2\text{P}_2$ has a higher T_c than LaFePO . Figure 1 (b) shows the Fermi surfaces of $\text{Ca}_4\text{Al}_2\text{O}_6\text{Fe}_2\text{P}_2$ in an undoped case and doped cases with ± 0.1 electrons per Fe atom within the rigid band approximation. Another noticeable difference is seen in the height of pnictogen (Pn) p bands at M . The top of P p bands in $\text{Ca}_4\text{Al}_2\text{O}_6\text{Fe}_2\text{P}_2$ lies close to -1.3 eV at M , whereas that of As p bands is not at M and those bands are below -1.9 eV.

To analyze the differences between the two compounds, the Wannier function technique is useful, since it enables us to evaluate the effective parameters of low-energy electronic states.³⁴⁾ We constructed maximally localized Wannier functions from the ten Fe d bands (d model) and plotted the interpolated band dispersion as curves in Fig. 1(a). It is found that the Wannier functions accurately reproduce the DFT-GGA band structures near the Fermi level. The Wannier function of the Fe $d_{X^2-Y^2}(d_{xy})$ orbital in $\text{Ca}_4\text{Al}_2\text{O}_6\text{Fe}_2\text{P}_2$ is shown in Fig. 1(c). [The X - and Y -axes refer to the conventional unit cell containing two Fe atoms, whereas the rotation of them by 45° defines the x - and y -axes. (see Fig. 2)] Although the shape of this Wannier function is mainly of the $d_{X^2-Y^2}$ character, it involves contributions from P p orbitals. We observed that the positive (blue) lobe of the $d_{X^2-Y^2}$ orbital is pushed down the c direction to hybridize with the P p orbitals below the Fe layer, while the negative (yellow) lobe is pushed up to hybridize with the P p orbitals above, as shown in Fig. 1(c). We confirmed that the shape of the corresponding Wannier function in $\text{Ca}_4\text{Al}_2\text{O}_6\text{Fe}_2\text{As}_2$ (not shown) has smaller contributions from the As p orbitals. This reflects (i) the Fe-P distance, which is smaller than the Fe-As distance, and (ii) the energy separation of the Fe d and the As p bands in $\text{Ca}_4\text{Al}_2\text{O}_6\text{Fe}_2\text{As}_2$, which is larger than that of the Fe d and the P p bands in $\text{Ca}_4\text{Al}_2\text{O}_6\text{Fe}_2\text{P}_2$.

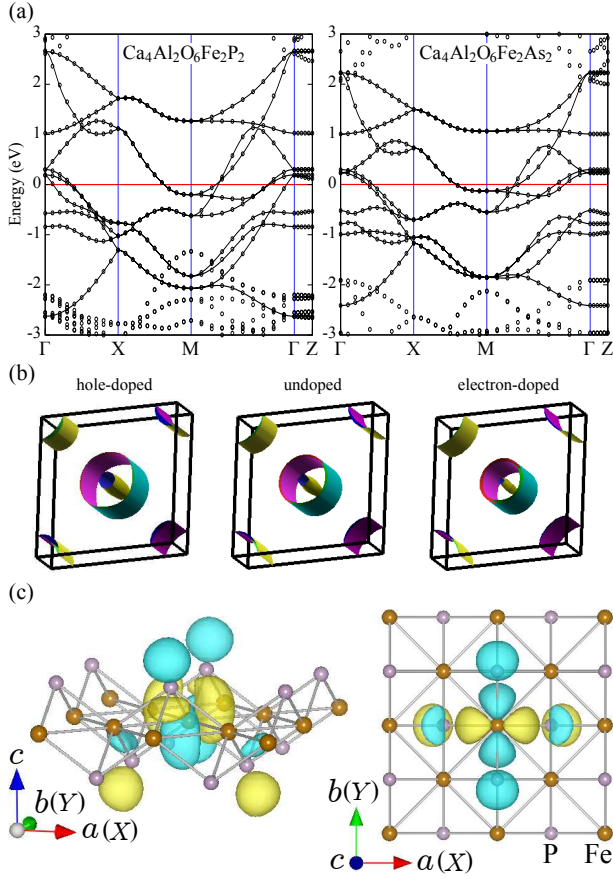


Fig. 1. (Color) (a) Nonmagnetic electronic band structures of $\text{Ca}_4\text{Al}_2\text{O}_6\text{Fe}_2\text{P}_2$ and $\text{Ca}_4\text{Al}_2\text{O}_6\text{Fe}_2\text{As}_2$. Circles represent DFT-GGA bands and curves represent bands interpolated using the maximally localized Wannier functions of d models. The origins of energy are set to the respective Fermi levels. (b) Fermi surfaces for hole-doped (left), undoped (middle), and electron-doped (right) $\text{Ca}_4\text{Al}_2\text{O}_6\text{Fe}_2\text{P}_2$. (c) A bird's-eye view of maximally localized Wannier function of Fe $d_{X^2-Y^2}$ orbital is shown on the left. The Wannier function viewed along the c axis is shown on the right. The a and b directions are parallel to the X - and Y -axes, respectively. Brown and purple balls represent Fe and P atoms, respectively. These figures were drawn with VESTA.³⁵⁾

To simplify the analysis of the electronic band structure, we unfolded the interpolated 10-band dispersion of d models following the procedure proposed by Kuroki *et al.*⁷⁾ The resultant 5-band structures obtained with the lattice parameters and the atomic coordinates fixed, while varying the chemical composition of the system, are shown in Fig. 3. It is found that the overall band structures with the same crystal structure look quite similar, especially in the vicinity of the Fermi level. For the $\text{Ca}_4\text{Al}_2\text{O}_6\text{Fe}_2\text{P}_2$ ($\text{Ca}_4\text{Al}_2\text{O}_6\text{Fe}_2\text{As}_2$) crystal structure, there exist three (two) Fermi surfaces around Γ in the original Brillouin zone irrespective of chemical composition, which correspond to the two (one) α hole pockets around $(0,0)$ and one γ hole pocket around (π,π) , as shown in Fig. 3. The numbers of Fermi surfaces around $(0,0)$ and (π,π) in the unfolded Brillouin zone for $\text{Ca}_4\text{Al}_2\text{O}_6\text{Fe}_2\text{As}_2$ and $\text{Ca}_4\text{Al}_2\text{O}_6\text{Fe}_2\text{P}_2$ with their own crystal structures are summarized in Table I. We observe in Fig. 3 that the calculated band widths of d

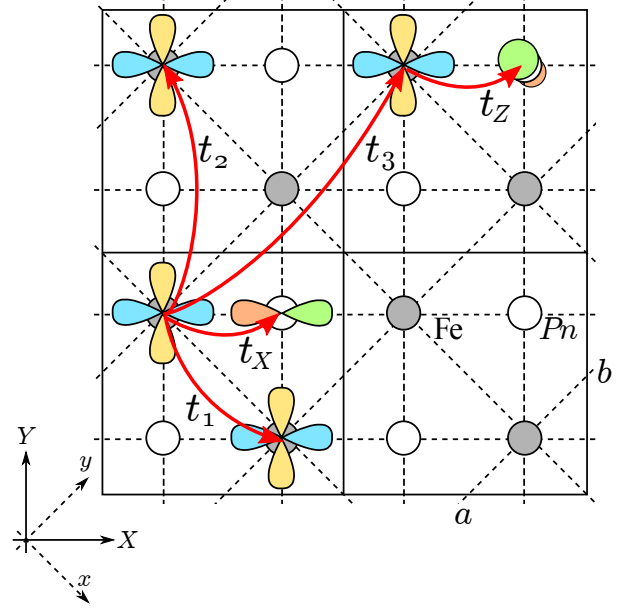


Fig. 2. (Color online) Schematic illustration of transfer integrals of a dpp model. Solid lines represent unit cells. Fe $d_{X^2-Y^2}$ orbitals and Pn p_X and p_Z orbitals are shown. We define the x - and y -axes by rotating the original X - and Y -axes by 45° . Transfer integrals are shown as red arrows. t_i ($i = 1, 2, 3$) is that between the $d_{X^2-Y^2}$ orbitals at the i -th nearest neighbors, while t_j ($j = X, Z$) is that between the p_j orbital and its nearest-neighboring $d_{X^2-Y^2}$ orbital.

models for $\text{Ca}_4\text{Al}_2\text{O}_6\text{Fe}_2\text{As}_2$ with the $\text{Ca}_4\text{Al}_2\text{O}_6\text{Fe}_2\text{As}_2$ and $\text{Ca}_4\text{Al}_2\text{O}_6\text{Fe}_2\text{P}_2$ crystal structures are 4.64 and 5.68 eV, respectively. Those for $\text{Ca}_4\text{Al}_2\text{O}_6\text{Fe}_2\text{As}_2$ and $\text{Ca}_4\text{Al}_2\text{O}_6\text{Fe}_2\text{P}_2$ crystal structures are 4.29 and 5.28 eV, respectively. The $\text{Ca}_4\text{Al}_2\text{O}_6\text{Fe}_2\text{P}_2$ crystal structure gave a larger band width than the $\text{Ca}_4\text{Al}_2\text{O}_6\text{Fe}_2\text{As}_2$ crystal structure when the same chemical composition was used, since the former has a smaller a and a smaller h_{Pn} . On the other hand, the $\text{Ca}_4\text{Al}_2\text{O}_6\text{Fe}_2\text{P}_2$ composition gave a smaller band width than the $\text{Ca}_4\text{Al}_2\text{O}_6\text{Fe}_2\text{As}_2$ composition when the same crystal structure was used, since the ion radius of the P atom is smaller than that of the As atom.

Table I. Numbers of Fermi surfaces around $(0,0)$ and (π,π) in unfolded Brillouin zone for $\text{Ca}_4\text{Al}_2\text{O}_6\text{Fe}_2\text{As}_2$ and $\text{Ca}_4\text{Al}_2\text{O}_6\text{Fe}_2\text{P}_2$. Those for LaFeAsO and LaFePO are also shown for comparison.

	$(0,0)$	(π,π)
$\text{Ca}_4\text{Al}_2\text{O}_6\text{Fe}_2\text{As}_2$	1	1
$\text{Ca}_4\text{Al}_2\text{O}_6\text{Fe}_2\text{P}_2$	2	1
LaFeAsO	2	1
LaFePO	2	0

It was demonstrated in our previous work²⁴⁾ that the Fe $d_{X^2-Y^2}$ (d_{xy}) orbital plays an important role in the band rearrangement of $\text{Ca}_4\text{Al}_2\text{O}_6\text{Fe}_2\text{As}_2$ when the local geometry of the FePn_4 tetrahedron is varied. For the quantitative analysis of the electronic structure of

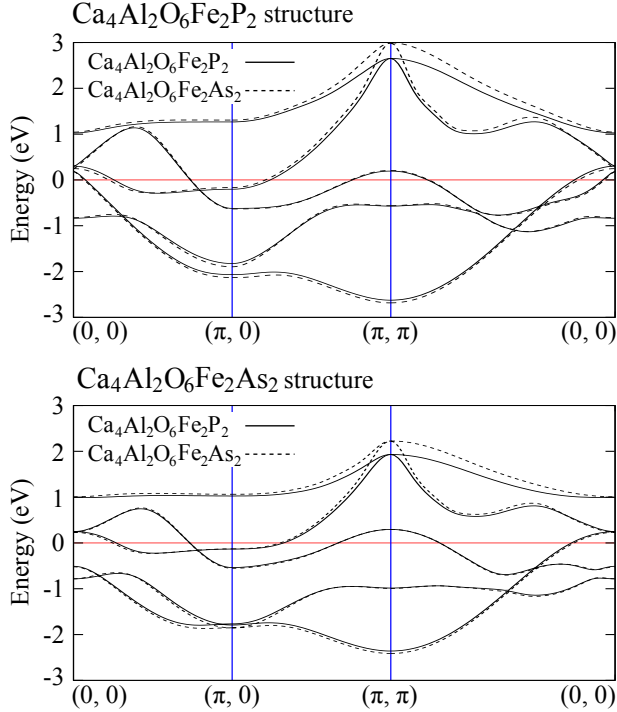


Fig. 3. (Color online) Unfolded 5-band structures of d models for $\text{Ca}_4\text{Al}_2\text{O}_6\text{Fe}_2\text{P}_2$ and $\text{Ca}_4\text{Al}_2\text{O}_6\text{Fe}_2\text{As}_2$ as solid and dashed curves, respectively. The upper (lower) panel shows the band structures obtained using the crystal structure of $\text{Ca}_4\text{Al}_2\text{O}_6\text{Fe}_2\text{P}_2$ ($\text{Ca}_4\text{Al}_2\text{O}_6\text{Fe}_2\text{As}_2$). The origins of energy are set to the respective Fermi levels.

$\text{Ca}_4\text{Al}_2\text{O}_6\text{Fe}_2\text{P}_2$ along this line, we constructed dpp models of the four systems mentioned above and examined how their chemical composition and crystal structures affect the electronic band structures. Each of the dpp models consists of 10 Fe d , 6 Pn p , and 18 O p orbitals. The transfer integrals and orbital energies of the $d_{X^2-Y^2}$ orbitals, which are equivalent to the xy orbitals, and the Pn p orbitals are shown in Table II. Although $|t_1| \gg |t_2|$ in the dpp models, t_1 in the d models are small in magnitude; consequently, t_1 and t_2 are comparable in the d models. Although the Wannier functions in the d model are spatially extended and have considerable weight at the pnictogen site, the d Wannier functions in the dpp model are localized and atomic-orbital-like.^{36,37} Hence, we can say that t_1 in the dpp model contains only direct hopping between the neighboring Fe sites, whereas t_1 in the d model contains indirect hopping via the pnictogen site as well.²⁴ This indicates that the indirect electron hopping of Fe- Pn -Fe partly cancels the direct hopping between the nearest-neighbor $d_{X^2-Y^2}$ orbitals. In the comparison of dpp t 's for the same chemical composition but different crystal structures, the difference between t_i ($i = 1, 2$)'s is small compared with their amplitudes. On the other hand, t_X and t_Z are much larger in the $\text{Ca}_4\text{Al}_2\text{O}_6\text{Fe}_2\text{P}_2$ crystal structure than in the $\text{Ca}_4\text{Al}_2\text{O}_6\text{Fe}_2\text{As}_2$ crystal structure for both chemical compositions. This is because the hybridization between the $d_{X^2-Y^2}$ and p orbitals is stronger for a smaller h_{Pn} . Since t_X and t_Z in the dpp models can

be regarded to be incorporated into t 's in the d models, the differences in band dispersion between the systems with the same chemical composition but different crystal structures come from the differences between the indirect hopping of Fe- Pn -Fe. The two-dimensional shape of the $d_{X^2-Y^2}$ orbital allows a larger hybridization with the p_Z orbital than with the p_X orbital, leading to t_Z much larger than t_X for all the four systems. In the comparison of dpp t 's for the same crystal structure but different chemical compositions, those for $\text{Ca}_4\text{Al}_2\text{O}_6\text{Fe}_2\text{As}_2$ are basically larger than those for $\text{Ca}_4\text{Al}_2\text{O}_6\text{Fe}_2\text{P}_2$ owing to the ion radius of the As atom larger than that of the P atom. t_X is, however, larger in $\text{Ca}_4\text{Al}_2\text{O}_6\text{Fe}_2\text{P}_2$ than in $\text{Ca}_4\text{Al}_2\text{O}_6\text{Fe}_2\text{As}_2$ if their crystal structures are the same. This is probably because the p electrons of a Pn atom are depleted for the hybridization between the p_Z orbital and its neighboring $d_{X^2-Y^2}$ orbitals.

As clarified above, the differences between the band structures of $\text{Ca}_4\text{Al}_2\text{O}_6\text{Fe}_2\text{P}_2$ and $\text{Ca}_4\text{Al}_2\text{O}_6\text{Fe}_2\text{As}_2$ with their own crystal structures, shown in Fig. 1(a), originate mainly not from the difference in chemical composition, but from that in pnictogen height. By defining the contribution t_1^{ind} from the indirect hopping Fe- Pn -Fe as the difference between the t_1 's of the d and dpp models ($t_1^{\text{ind}} \equiv t_1^d - t_1^{\text{dpp}}$), we can estimate t_1^{ind} to be 0.462 eV in $\text{Ca}_4\text{Al}_2\text{O}_6\text{Fe}_2\text{P}_2$ and 0.337 eV in $\text{Ca}_4\text{Al}_2\text{O}_6\text{Fe}_2\text{As}_2$. In our previous work,²⁴ we estimated t_1^{ind} for LaFeAsO ($h_{\text{As}} = 1.319 \text{ \AA}$) to be 0.394 eV. These values are reasonable because a smaller h_{Pn} gives a larger t_1^{ind} for these three systems. The direct hopping of LaFeAsO , $t_1^{\text{dpp}} = -0.243 \text{ eV}$, is much smaller than those of $\text{Ca}_4\text{Al}_2\text{O}_6\text{Fe}_2\text{P}_2$ and $\text{Ca}_4\text{Al}_2\text{O}_6\text{Fe}_2\text{As}_2$, which is due to the larger a of LaFeAsO .

Table II. Orbital energies and transfer integrals (in eV) of Fe $d_{X^2-Y^2}$ and Pn p Wannier orbitals of dpp models. The descriptions P and As indicate $\text{Ca}_4\text{Al}_2\text{O}_6\text{Fe}_2\text{P}_2$ and $\text{Ca}_4\text{Al}_2\text{O}_6\text{Fe}_2\text{As}_2$, respectively, for the chemical composition and crystal structure. Transfer integrals obtained from d models are also shown in parentheses. The origins of orbital energies ε are set to the respective Fermi levels.

Composition	Crystal structure			
	P	As		
P	$\varepsilon_{X^2-Y^2}$	-0.977(0.023)	-0.854(-0.204)	
	t_1	-0.370(0.092)	-0.362(-0.044)	
	t_2	-0.080(0.119)	-0.080(0.065)	
	t_3	-0.014(-0.025)	-0.011(-0.009)	
	ε_X	-2.491	-2.383	
	ε_Z	-2.537	-2.846	
	t_X	0.153	0.069	
	t_Z	-0.646	-0.537	
	As	$\varepsilon_{X^2-Y^2}$	-1.000(0.047)	-0.882(-0.197)
		t_1	-0.387(0.102)	-0.374(-0.037)
t_2		-0.089(0.121)	-0.087(0.067)	
t_3		-0.015(-0.030)	-0.011(-0.012)	
ε_X		-2.496	-2.391	
ε_Z		-2.566	-2.889	
t_X		0.128	0.053	
t_Z		-0.666	-0.552	

3.2 Alloying effect on $\text{Ca}_4\text{Al}_2\text{O}_6\text{Fe}_2\text{AsP}$

To study whether or not even the electronic structure of a system in which P and As coexist is determined mainly by crystal structure, we unfolded the band structures and compared them in the three cases of $\text{Ca}_4\text{Al}_2\text{O}_6\text{Fe}_2(\text{As}_{1-x}\text{P}_x)_2$: $\text{Ca}_4\text{Al}_2\text{O}_6\text{Fe}_2\text{P}_2$ ($x = 1$), $\text{Ca}_4\text{Al}_2\text{O}_6\text{Fe}_2\text{As}_2$ ($x = 0$), and $\text{Ca}_4\text{Al}_2\text{O}_6\text{Fe}_2\text{AsP}$ ($x = 0.5$). For the $x = 1$ and 0 systems, the average crystal structure of $\text{Ca}_4\text{Al}_2\text{O}_6\text{Fe}_2\text{P}_2$ and $\text{Ca}_4\text{Al}_2\text{O}_6\text{Fe}_2\text{As}_2$ was used. The fractional height of the pnictogen atoms used is thus $z_{\text{Pn}} = 0.0924$. For the $x = 0.5$ system, we used a $\sqrt{2} \times \sqrt{2} \times 1$ supercell containing four Fe atoms [see Fig. 4(a)]. The lattice parameters and atomic coordinates except P and As were set to the same as those for the $x = 1$ and 0 systems. The P and As atoms were set at the experimental heights in $\text{Ca}_4\text{Al}_2\text{O}_6\text{Fe}_2\text{P}_2$ ($h_{\text{P}} = 1.306$ Å) and $\text{Ca}_4\text{Al}_2\text{O}_6\text{Fe}_2\text{As}_2$ ($h_{\text{As}} = 1.500$ Å), respectively. The fractional height of the pnictogen atoms used are thus $z_{\text{P}} = 0.0861$ and $z_{\text{As}} = 0.0989$. The dimensions $\sqrt{2} \times \sqrt{2} \times 1$ of the supercell are the smallest needed for the realization of equal distributions of the two atomic species above and below the Fe layer. We unfolded the Fe d bands of the $x = 0.5$ system using eq. (1). Specifically, we first constructed 20 maximally localized Wannier functions of the Fe d character and then unfolded the interpolated band structure by regarding the supercell as consisting of four primitive cells, each of which contains one Fe site: $\mathbf{a}_{\text{sc}} = 2\mathbf{a}_{\text{pc}}$, $\mathbf{b}_{\text{sc}} = 2\mathbf{b}_{\text{pc}}$, and $\mathbf{c}_{\text{sc}} = \mathbf{c}_{\text{pc}}$. We provide in Fig. 4(b) the unfolded band structure for the $x = 0.5$ system as blurred curves and that obtained by fixing the weights of the delta functions in eq. (1) constant as solid curves. It is clearly seen that the unfolded band structure is essentially 20-fold and that the weights of the delta functions, however, make five of them noticeable for almost all the wave vectors. The unfolded band dispersion of the $x = 0.5$ system exhibits different features along the two paths, one from $(\pi, 0)$ to (π, π) (corresponding to wave vectors along the b direction) and the other from $(0, \pi)$ to (π, π) (corresponding to wave vectors along the a direction), owing to the inequivalence of the a and b directions [see Fig. 4(a)]. Noticeable gap openings of three of the unfolded bands are seen on the latter path, while the continuity of the unfolded bands on the former path looks firmer. They originate from the difference between the arrangement of atoms of different species along the a direction, and that of the same species along the b direction.

Figure 4(c) shows the unfolded band structures for the $x = 0, 1$, and 0.5 systems. Not only the unfolded band structures for the $x = 0$ and 1 systems, for which the exact unfolding is possible, but also that for the $x = 0.5$ system all look quite similar, especially in the vicinity of the Fermi levels, as well as in Fig. 3. We also confirmed that the band structure of $\text{Ca}_4\text{Al}_2\text{O}_6\text{Fe}_2\text{P}_2$ ($\text{Ca}_4\text{Al}_2\text{O}_6\text{Fe}_2\text{As}_2$) with an average crystal structure except for the P (As) atom with its experimental height has three (two) Fermi surfaces around Γ . This indicates that pnictogen height is a crucial factor for the multiplicity of Fermi surfaces around Γ . It is interesting to see the proximity of the Fermi level at $(0, 0)$ for the $x = 0.5$ sys-

tem [see Fig. 4(c)]. The top of the second-lowest unfolded band sits 0.2 eV below the Fermi level, which is well reproduced by the $x = 0$ and 1 systems with an average crystal structure despite the $x = 0.5$ system containing pnictogen height disorder. There is an atomic configuration for the chemical composition $x = 0.5$ using the conventional unit cell (see Fig. 2), in which the atoms of one of the two species are all located above the Fe layer and those of the other species below the layer. We also calculated the electronic band structure of this system (not shown) with the experimental pnictogen heights of the P and As atoms, and found that its unfolded bands near the Fermi level are accurately reproduced by the $x = 0$ and 1 systems, as shown in Fig. 4(c). These results corroborate the independence of the electronic structure of a $\text{Ca}_4\text{Al}_2\text{O}_6\text{Fe}_2(\text{As}_{1-x}\text{P}_x)_2$ system of the chemical composition. We expect an accurate calculation of a band structure near the Fermi level for an arbitrary x using a crystal structure modeled simply by linearly connecting the $\text{Ca}_4\text{Al}_2\text{O}_6\text{Fe}_2\text{P}_2$ and $\text{Ca}_4\text{Al}_2\text{O}_6\text{Fe}_2\text{As}_2$ crystal structures.

3.3 Generalized susceptibility of $\text{Ca}_4\text{Al}_2\text{O}_6\text{Fe}_2(\text{As}_{1-x}\text{P}_x)_2$

Given the results obtained above, we calculated the generalized susceptibility χ_0 of $\text{Ca}_4\text{Al}_2\text{O}_6\text{Fe}_2\text{P}_2$ and $\text{Ca}_4\text{Al}_2\text{O}_6\text{Fe}_2\text{As}_2$ with gradually varying their crystal structures. We expect that the χ_0 calculated in such a way accurately reproduces the qualitative behavior of $\text{Ca}_4\text{Al}_2\text{O}_6\text{Fe}_2(\text{As}_{1-x}\text{P}_x)_2$ for arbitrary x . The lattice parameters and atomic coordinates c used are linearly parametrized by the crystal structure ratio λ as $c(\lambda) = \lambda c_{\text{P}} + (1 - \lambda)c_{\text{As}}$. $\lambda = 0$ and 1 correspond to the $\text{Ca}_4\text{Al}_2\text{O}_6\text{Fe}_2\text{As}_2$ and $\text{Ca}_4\text{Al}_2\text{O}_6\text{Fe}_2\text{P}_2$ crystal structures, respectively. We calculated $\chi_0(\mathbf{q})$ using eq. (2) and plotted it in Fig. 5(a) for $\text{Ca}_4\text{Al}_2\text{O}_6\text{Fe}_2\text{As}_2$ and $\text{Ca}_4\text{Al}_2\text{O}_6\text{Fe}_2\text{P}_2$ with $\lambda = 0, 0.5$, and 1. Those in doped cases with ± 0.1 electrons per Fe atom with the rigid band approximation are also shown. The plotted χ_0 is seen to be sensitive to the difference in chemical composition compared with the band energy. The peaks of χ_0 are located at M in the undoped cases of both $\text{Ca}_4\text{Al}_2\text{O}_6\text{Fe}_2\text{As}_2$ and $\text{Ca}_4\text{Al}_2\text{O}_6\text{Fe}_2\text{P}_2$, while, in the doped cases, the peaks are located at incommensurate \mathbf{q} 's close to M. We observe that the heights of the peaks are reduced by doping for both $\text{Ca}_4\text{Al}_2\text{O}_6\text{Fe}_2\text{As}_2$ and $\text{Ca}_4\text{Al}_2\text{O}_6\text{Fe}_2\text{P}_2$, which suggests that their magnetic instability is suppressed under doping. Figure 5(b) shows the $\chi_0(\text{M})$'s of $\text{Ca}_4\text{Al}_2\text{O}_6\text{Fe}_2\text{P}_2$ and $\text{Ca}_4\text{Al}_2\text{O}_6\text{Fe}_2\text{As}_2$ as functions of λ . Although the $\text{Ca}_4\text{Al}_2\text{O}_6\text{Fe}_2\text{P}_2$ systems with smaller band widths give a larger $\chi_0(\text{M})$ than the $\text{Ca}_4\text{Al}_2\text{O}_6\text{Fe}_2\text{As}_2$ systems, the qualitative behavior of monotonic decrease in $\chi_0(\text{M})$ for both $\text{Ca}_4\text{Al}_2\text{O}_6\text{Fe}_2\text{P}_2$ and $\text{Ca}_4\text{Al}_2\text{O}_6\text{Fe}_2\text{As}_2$ are found to be the same in the entire range of λ . We found that, with increasing λ , the number of the α Fermi surfaces around $(0, 0)$ increases from one to two near $\lambda = 0.75$ for both $\text{Ca}_4\text{Al}_2\text{O}_6\text{Fe}_2\text{P}_2$ and $\text{Ca}_4\text{Al}_2\text{O}_6\text{Fe}_2\text{As}_2$. The larger number of Fermi surfaces for $\lambda > 0.75$ would be preferable to larger χ_0 because of the larger number of scattering channels. The

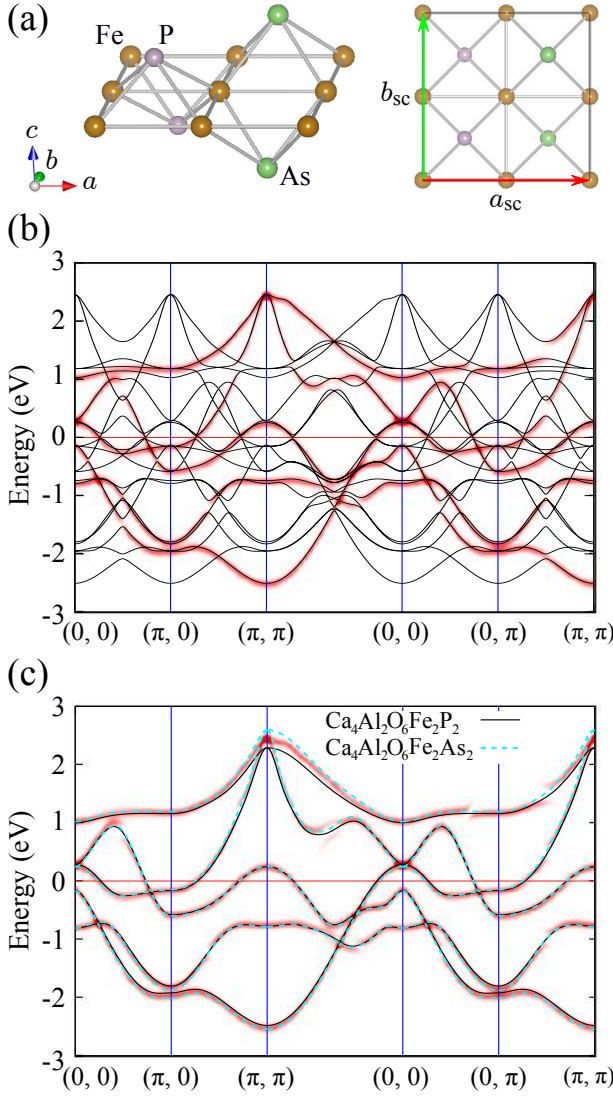


Fig. 4. (Color) (a) Bird's-eye view of an Fe layer of a $\sqrt{2} \times \sqrt{2} \times 1$ supercell for an $x = 0.5$ structure is shown on the left. The layer viewed along the c -axis is shown on the right, together with the primitive lattice vectors of the supercell. Brown, purple, and green balls represent Fe, P, and As atoms, respectively. (b) The blurred curves are for the unfolded 20 bands of the d model for the $x = 0.5$ system using the supercell. The solid curves represent the unfolded bands with weights of delta functions fixed constant. The coordinates of high-symmetry points are with respect to the primitive reciprocal lattice vectors of the primitive cell. (c) Unfolded band structures of $x = 1, 0.5$, and 0 systems. The solid and dashed curves are for the 5-band structures of the $x = 1$ and 0 systems, respectively, with the crystal structure fixed at the average of $\text{Ca}_4\text{Al}_2\text{O}_6\text{Fe}_2\text{P}_2$ and $\text{Ca}_4\text{Al}_2\text{O}_6\text{Fe}_2\text{As}_2$. The origins of energy are set to the respective Fermi levels.

calculated χ_0 , however, exhibits the trend of a monotonic decrease. To examine the factors determining this trend, we plot the band energies $E_{xy}(\pi, \pi)$ in Fig. 5(c) for the undoped systems as functions of λ . $E_{xy}(\pi, \pi)$ is the height of the $d_{X^2-Y^2}$ -derived band. As is shown, a smaller λ gives a higher $E_{xy}(\pi, \pi)$ and thus a more effective γ Fermi surface, and the difference in chemical composition has only a minor effect on the values of $E_{xy}(\pi, \pi)$. Furthermore, a smaller λ (a larger a and a larger h_{Pn}) leads to narrower bands and a larger density

of states. These observations suggest that the effects of a small λ overcome the difference in the number of α Fermi surfaces.

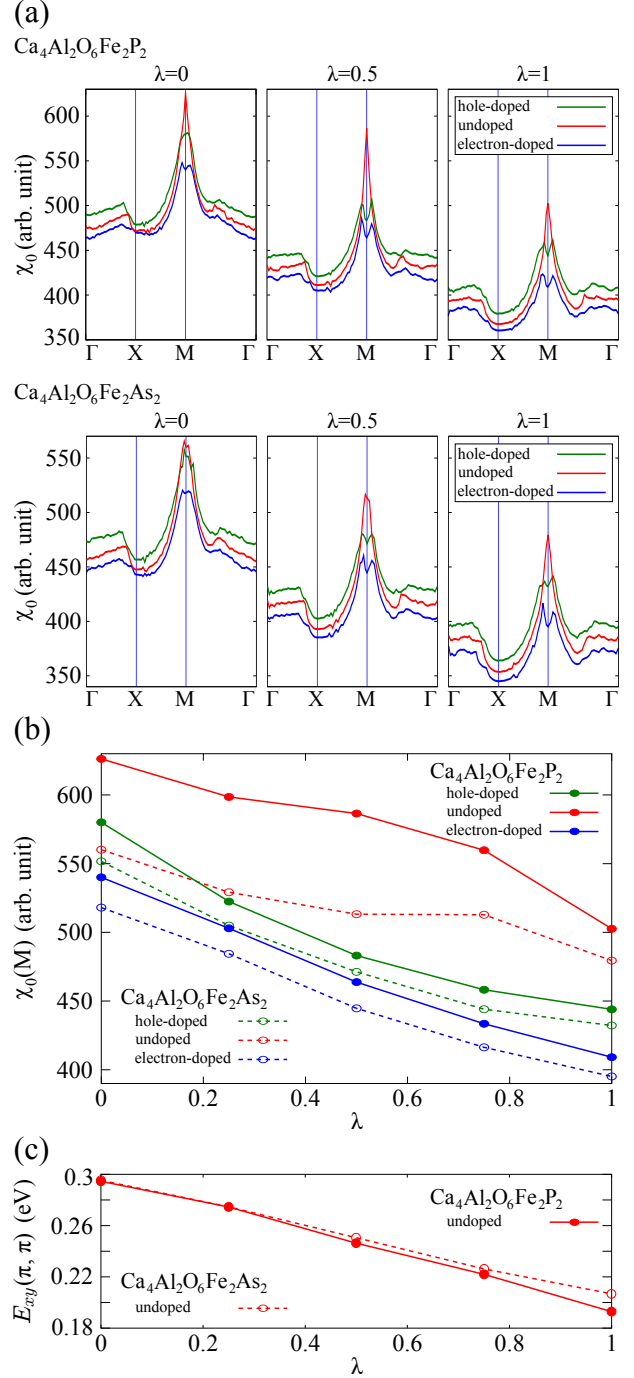


Fig. 5. (Color) (a) Generalized susceptibilities $\chi_0(\mathbf{q})$ of $\text{Ca}_4\text{Al}_2\text{O}_6\text{Fe}_2\text{P}_2$ and $\text{Ca}_4\text{Al}_2\text{O}_6\text{Fe}_2\text{As}_2$ for crystal structure ratios $\lambda = 0, 0.5$ and 1 . Those in doped cases are also shown. (b) $\chi_0(M)$ in doped and undoped cases of $\text{Ca}_4\text{Al}_2\text{O}_6\text{Fe}_2\text{P}_2$ and $\text{Ca}_4\text{Al}_2\text{O}_6\text{Fe}_2\text{As}_2$ as functions of λ . (c) Band energies of $d_{X^2-Y^2}$ -derived bands at (π, π) for undoped systems.

4. Conclusions

We performed first-principles calculations of the electronic structures of $\text{Ca}_4\text{Al}_2\text{O}_6\text{Fe}_2\text{P}_2$ and

$\text{Ca}_4\text{Al}_2\text{O}_6\text{Fe}_2\text{As}_2$. $\text{Ca}_4\text{Al}_2\text{O}_6\text{Fe}_2\text{P}_2$ ($\text{Ca}_4\text{Al}_2\text{O}_6\text{Fe}_2\text{As}_2$) was found to have three (two) Fermi surfaces around Γ . We found that the systems of the same crystal structure but different chemical compositions give rise to similar band structures. By constructing the maximally localized Wannier functions and analyzing their transfer integrals, we demonstrated that the differences between the band structures of $\text{Ca}_4\text{Al}_2\text{O}_6\text{Fe}_2\text{P}_2$ and $\text{Ca}_4\text{Al}_2\text{O}_6\text{Fe}_2\text{As}_2$ originate mainly from the difference in pnictogen height. Specifically, the hybridization between the p_Z orbital and its neighboring $d_{X^2-Y^2}$ orbitals plays important roles in determining the electronic structures.

We analyzed the electronic structure of $\text{Ca}_4\text{Al}_2\text{O}_6\text{Fe}_2\text{AsP}$ by unfolding its electronic bands. We found that its band structure resembles the band structures of $\text{Ca}_4\text{Al}_2\text{O}_6\text{Fe}_2\text{P}_2$ and $\text{Ca}_4\text{Al}_2\text{O}_6\text{Fe}_2\text{As}_2$ with an average crystal structure, although $\text{Ca}_4\text{Al}_2\text{O}_6\text{Fe}_2\text{AsP}$ contains pnictogen height disorder. We therefore expected that an accurate calculation of band structures for an arbitrary x is possible using a crystal structure modeled by linearly connecting the crystal structures of $\text{Ca}_4\text{Al}_2\text{O}_6\text{Fe}_2\text{P}_2$ and $\text{Ca}_4\text{Al}_2\text{O}_6\text{Fe}_2\text{As}_2$.

We then calculated the generalized susceptibility χ_0 for $\text{Ca}_4\text{Al}_2\text{O}_6\text{Fe}_2(\text{As}_{1-x}\text{P}_x)_2$ using crystal structures constructed from the linear interpolation of the crystal structures of $\text{Ca}_4\text{Al}_2\text{O}_6\text{Fe}_2\text{P}_2$ and $\text{Ca}_4\text{Al}_2\text{O}_6\text{Fe}_2\text{As}_2$. It was found that a smaller crystal structure ratio λ leads to a larger χ_0 because of the larger density of states and the more effective γ Fermi surface.

Further theoretical and experimental investigations of the structural and magnetic properties of perovskite-type systems are required to clarify and optimize the superconducting properties of such systems.

Acknowledgement

We thank Professor K. Terakura for discussions. We also thank Dr. A. Iyo, Dr. H. Eisaki, Dr. C. H. Lee, Dr. P. M. Shirage, Dr. K. Kihou, and Dr. H. Kito for discussions and for providing us with experimental data prior to publication. This work was partly supported by the Strategic International Collaborative Research Program (SICORP), Japan Science and Technology Agency, by the Next Generation Super Computing Project, Nanoscience Program, and by a Grant-in-Aid for Scientific Research on Innovative Areas, "Materials Design through Computics: Complex Correlation and Non-Equilibrium Dynamics" (No. 22104010) from MEXT, Japan. The calculations were performed using computational facilities at TACC, AIST as well as at the Supercomputer Center of ISSP and at the Information Technology Center, both at the University of Tokyo.

- 1) Y. Kamihara, H. Hiramatsu, M. Hirano, R. Kawamura, H. Yanagi, T. Kamiya, and H. Hosono: *J. Am. Chem. Soc.* **128** (2006) 10012.
- 2) Y. Kamihara, T. Watanabe, M. Hirano, and H. Hosono: *J. Am. Chem. Soc.* **130** (2008) 3296.
- 3) Z.-A. Ren, W. Lu, J. Yang, W. Yi, X. L. Shen, Z. C. Li, G. C. Che, X. L. Dong, L. L. Sun, F. Zhou, and Z. X. Zhao, *Chin. Phys. Lett.* **25** (2008) 2215.
- 4) D. J. Singh and M.-H. Du: *Phys. Rev. Lett.* **100** (2008) 237003.
- 5) I. I. Mazin, D. J. Singh, M. D. Johannes, and M. H. Du: *Phys. Rev. Lett.* **101** (2008) 057003.
- 6) S. Ishibashi, K. Terakura, and H. Hosono: *J. Phys. Soc. Jpn.* **77** (2008) 053709.
- 7) K. Kuroki, S. Onari, R. Arita, H. Usui, Y. Tanaka, H. Kontani, and H. Aoki: *Phys. Rev. Lett.* **101** (2008) 087004.
- 8) C. H. Lee, A. Iyo, H. Eisaki, H. Kito, M. T. Fernandez-Diaz, T. Ito, K. Kihou, H. Matsuhata, M. Braden, and K. Yamada: *J. Phys. Soc. Jpn.* **77** (2008) 083704.
- 9) V. Vildosola, L. Pourovskii, R. Arita, S. Biermann, and A. Georges: *Phys. Rev. B* **78** (2008) 064518.
- 10) K. Kuroki, H. Usui, S. Onari, R. Arita, and H. Aoki: *Phys. Rev. B* **79** (2009) 224511.
- 11) Y. Mizuguchi, Y. Hara, K. Deguchi, S. Tsuda, T. Yamaguchi, K. Takeda, H. Kotegawa, H. Tou, and Y. Takano: *Supercond. Sci. Technol.* **23** (2010) 054013 and references therein.
- 12) Y. Mizuguchi and Y. Takano: *J. Phys. Soc. Jpn.* **79** (2010) 102001.
- 13) H. Ogino, Y. Matsumura, Y. Katsura, K. Ushiyama, S. Horii, K. Kishio, and J. Shimoyama: *Supercond. Sci. Technol.* **22** (2009) 075008.
- 14) X. Zhu, F. Han, G. Mu, P. Cheng, B. Shen, B. Zeng, and H. Wen: *Phys. Rev. B* **79** (2009) 220512.
- 15) H. Kotegawa, T. Kawazoe, H. Tou, K. Murata, H. Ogino, K. Kishio, and J. Shimoyama: *J. Phys. Soc. Jpn.* **78** (2009) 123707.
- 16) S. Sato, H. Ogino, N. Kawaguchi, Y. Katsura, K. Kishio, J. Shimoyama, H. Kotegawa, and H. Tou: *Supercond. Sci. Technol.* **23** (2010) 045001.
- 17) N. Kawaguchi, H. Ogino, Y. Shimizu, K. Kishio, and J. Shimoyama: *Appl. Phys. Express* **3** (2010) 063102.
- 18) H. Ogino, S. Sato, K. Kishio, J. Shimoyama, T. Tohei, and Y. Ikuhara: *Appl. Phys. Lett.* **97** (2010) 072506.
- 19) H. Ogino, Y. Shimizu, K. Ushiyama, N. Kawaguchi, K. Kishio, and J. Shimoyama: *Appl. Phys. Express* **3** (2010) 063103.
- 20) P. M. Shirage, K. Kihou, C. H. Lee, H. Kito, H. Eisaki, and A. Iyo: *Appl. Phys. Lett.* **97** (2010) 172506.
- 21) H. Ogino, K. Machida, A. Yamamoto, K. Kishio, J. Shimoyama, T. Tohei, and Y. Ikuhara: *Supercond. Sci. Technol.* **23** (2010) 115005.
- 22) P. M. Shirage, K. Kihou, C. H. Lee, H. Kito, H. Eisaki, and A. Iyo: *J. Am. Chem. Soc.* **133** (2011) 9630.
- 23) H. Ogino, Y. Shimizu, N. Kawaguchi, K. Kishio, J. Shimoyama, T. Tohei, and Y. Ikuhara: *Supercond. Sci. Technol.* **24** (2011) 085020.
- 24) T. Miyake, T. Kosugi, S. Ishibashi, and K. Terakura: *J. Phys. Soc. Jpn.* **79** (2010) 123713.
- 25) H. Usui and K. Kuroki: *Phys. Rev. B* **84** (2011) 024505.
- 26) N. Marzari and D. Vanderbilt: *Phys. Rev. B* **56** (1997) 12847; I. Souza, N. Marzari, and D. Vanderbilt: *Phys. Rev. B* **65** (2001) 035109.
- 27) <http://www.qmas.jp/>
- 28) P. E. Blöchl: *Phys. Rev. B* **50** (1994) 17953.; G. Kresse and D. Joubert: *Phys. Rev. B* **59** (1999) 1758.
- 29) S. Ishibashi and K. Terakura: *Proc. Int. Symp. Fe-Pnictide Superconductors*, *J. Phys. Soc. Jpn.* **77** (2008) Suppl. C, p. 91.
- 30) S. Ishibashi and K. Terakura: *Physica C* **470** (2010) S336.
- 31) J. P. Perdew, K. Burke, and M. Ernzerhof: *Phys. Rev. Lett.* **77** (1996) 3865.
- 32) C. H. Lee, P. M. Shirage, K. Kihou, H. Kito, A. Iyo, and H. Eisaki: private communication. In the present work, we used the refined lattice parameters $a = 3.69277 \text{ \AA}$ and $c = 14.9270 \text{ \AA}$, which are slightly different from those previously reported.²⁰⁾
- 33) W. Ku, T. Berljin, and C. H. Lee: *Phys. Rev. Lett.* **104** (2010) 216401.
- 34) T. Miyake and F. Aryasetiawan: *Phys. Rev. B* **77** (2008) 085122; T. Miyake, F. Aryasetiawan and M. Imada: *Phys. Rev. B* **80** (2009) 155134.
- 35) K. Momma and F. Izumi: *J. Appl. Crystallogr.* **41** (2008) 653.
- 36) M. Aichhorn, L. Pourovskii, V. Vildosola, M. Ferrero, O. Parcollet, T. Miyake, A. Georges, and S. Biermann: *Phys. Rev. B* **80** (2009) 085101.

37) T. Miyake, K. Nakamura, R. Arita, and M. Imada: J. Phys. Soc. Jpn. **79** (2010) 044705.